PRAMANA
— journal of
physics

Vol. 68, No. 4
April 2007
pp. 547–569

Systematic study of spatiotemporal dynamics of intense femtosecond laser pulses in BK-7 glass

RAM GOPAL, V DEEPAK and S SIVARAMAKRISHNAN
Department of Physics, Sri Sathya Sai Institute of Higher Learning,
Prasanthi Nilayam 515 134, India
E-mail: srk.phy.psn@sssihl.edu.in; email2sivaram@gmail.com

MS received 20 June 2006; revised 5 November 2006; accepted 5 January 2007

Abstract. In this paper we present a systematic study of the spatial and temporal effects of intense femtosecond laser pulses in BK-7 over a broad range of input powers, 1–1000 times the critical power for self-focusing (P_{cr}) by numerically solving the nonlinear Schrödinger equation (NLS). Most numerical studies have not been extended to such high powers. A clear-cut classification of spatio-temporal dynamics up to very high powers into three regimes – the group-velocity dispersion (GVD) regime, the ionization regime and the dominant plasma regime – as done here, is a significant step towards a better understanding. Further, we examine in detail the role of GVD in channel formation by comparing BK-7 to an 'artificial' medium. Our investigations bring forth the important observation that diffraction plays a minimal role in the formation of multiple cones and that plasma plays a diffraction-like role at very high powers. A detailed study of the spatio-temporal dynamics in any condensed medium over this range of powers has not been reported hitherto, to the best of our knowledge. We also suggest appropriate operational powers for various applications employing BK-7 on the basis of our results.

Keywords. Self-focusing; channeling; filamentation; ultrafast processes; laser-plasmas.

PACS Nos 42.65.Re; 42.65.Sf; 52.35.Mw; 52.38.Hb

1. Introduction

The propagation of ultrashort intense laser pulses in condensed media, liquids and gases has evoked considerable interest due to many applications, potential and in vogue, like laser machining [1, 2], lightning control, atmospheric analysis and remote sensing of molecules [3] and supercontinuum generation [5–7]. The commercial availability of intense femtosecond lasers has made extensive experimental studies possible. A variety of far-field patterns have been demonstrated after propagation in nonlinear media by the use of periodic structures like a wire mesh [8,9]. Bulk modifications can be used to fabricate waveguides [10, 11], photonic crystals [12] and optical memories [13]. The control of propagation dynamics, both spatial and temporal, is crucial in these applications. This necessitates a complete

understanding of the physical processes that govern the spatio-temporal dynamics of the intense ultrashort pulse in the medium. At present, it is reasonable to say that the understanding of the interplay of various physical processes over the extensive range of various parameters like input power, pulse width, wavelength and repetition rate is far from complete. This is largely due to the fact that experimental conditions vary widely and models used are not always comprehensive. Thus, the physics of this problem needs further study.

The forerunner to all the effects seen in the propagation of the femtosecond laser pulses, is the intensity dependent refractive index (n_2). The effective refractive index of the medium of propagation becomes $n = n_0 + n_2 I$, where I is the intensity. For a pulse with a Gaussian spatial intensity profile, this leads to self-focusing. While diffraction concomitantly leads to a natural divergence, for input powers greater than the critical power for self-focusing $P_{\rm cr} = 1.22\pi\lambda_0/(32 n_0 n_2)$, the pulse undergoes a catastrophic collapse since self-focusing dominates diffraction [14,15]. Such a collapse is prevented by various processes which saturate self-focusing and arrest the build-up intensity. Even though the mechanisms involved in this process have been identified, no simple analytical model for the propagation of intense femtosecond pulses successfully explains this plethora of effects. Numerical models have been successful in explaining experimental observations often leading to succinct intuitive conclusions.

Having said this, we must add that most numerical studies have been done for input powers much lower than $1000P_{\rm cr}$. In each case spatio-temporal phenomena such as pulse splitting [16], pulse compression [17], self-channeling and formation of filaments [18], multiple refocusing [19] and multiple-cone structure [20] have been successfully explained for the case of each experimental situation. There is, clearly, a need for a comprehensive study extending over the entire range of 1–$1000P_{\rm cr}$ in order to provide a better understanding of the generic observations made over a wide variety of materials and laser parameters. In this paper we present the results based on solving the nonlinear Schrödinger equation [10] to explain many observations, generic and specific, over the range 1–$1000P_{\rm cr}$ in a condensed medium. While experiments have been performed [21] with input powers up to 1000 times the critical power for self-focusing, $P_{\rm cr}$, a comprehensive numerical study in the range 1–$1000P_{\rm cr}$ has not been undertaken to the best of our knowledge. We present here a study of the spatio-temporal dynamics in the power range of 1–$1000P_{\rm cr}$ in a condensed medium. A condensed medium is highly suitable for such a study due to nonlinear effects which occur after relatively short distances of propagation in condensed media when compared to gases and they also retain spatial features like damage tracks, which are washed away in a liquid.

The main contributions of this paper are as follows: Firstly, we make a successful attempt to systematize generic observations up to $1000P_{\rm cr}$ and propose a classification scheme. Secondly, we present a complete study of the spatio-temporal effects in BK-7 at very high powers. Thirdly, we examine the role of GVD in channel formation and bring to light the insignificant role of diffraction in multiple-cone formation due to the early onset of a sufficiently strong plasma. Another highlight of this paper, as is the case with some others [22], is that the NLS equation is solved numerically using a commercially available personal computer. Many groups use multinode computing machines to solve the NLS equation or Maxwell's equations

directly, to study the propagation of ultrashort pulses for more general cases. The ubiquitous personal computer can be used to gain valuable insights into the bigger and composite problem by judicious use of computational power and careful programming.

In §2, the necessary theory and the numerical model are developed. In §3, we present our results along with developing a comprehensive picture of the dynamics by suggesting a classification scheme.

2. Theory and numerical scheme

2.1 *Nonlinear Schrödinger equation*

The electric field of the pulse propagating along the $+z$-direction is written as

$$\tilde{E}(r,z,t') = E(r,z,t')\exp(i(k_0 z - \omega_0 t')), \tag{1}$$

where $\tilde{E}(r,z,t')$ is expressed in cylindrical polar coordinates and is a product of the pulse envelope $E(r,z,t')$ and the harmonic part $\exp(i(k_0 z - \omega_0 t'))$. For the cases to be considered, the variation of the former is slower than the latter, leading to the slowly-varying envelope approximation (SVEA). As a consequence of this approximation, the equation for propagation for the pulse envelope can be reduced to the nonlinear Schrödinger (NLS) equation from the wave equation using well-known arguments [14,15,23]. In a frame of reference that moves with the center of the pulse at the group velocity v_{g}, the NLS equation becomes

$$\begin{aligned}&\frac{\partial E}{\partial z} + \frac{i}{2}\beta_2 \frac{\partial^2 E}{\partial t^2} - \beta_3 \frac{\partial^3 E}{\partial t^3} - \frac{i}{2n_0 k_0}\left(1 - \frac{i}{\omega_0}\frac{\partial}{\partial t}\right)\left(\frac{\partial^2}{\partial r^2} + \frac{1}{r}\frac{\partial}{\partial r}\right)E \\ &= i n_2 k_0 \left(1 + \frac{i}{\omega_0}\frac{\partial}{\partial t}\right)(|E|^2 E).\end{aligned} \tag{2}$$

The variable t is the retarded time and is related to the time coordinate t' of the stationary frame by $t = t' - v_{\mathrm{g}} z^{-1}$. In the above equation, E is normalized so that $|E|^2$ equals the intensity of the pulse in W/cm^2. The terms with β_2 and β_3 as coefficients account for second- and third-order group velocity dispersions (GVD), respectively. The first-order GVD term is absent since we are working in the frame of reference moving at the group velocity of the pulse. The subsequent term on the left-hand side is the space-time focusing term in which the transverse Laplacian leads to familiar diffraction effects. On the right-hand side the first term accounts for third-order nonlinear effects due to the intensity dependent refractive index n_2. Self-focusing in space and self-phase modulation (SPM) in time are direct consequences of this term [14,15,23]. The partial time derivative in the term causes self-steepening, which leads to the formation of a shock front in the pulse envelope. While SPM is responsible for symmetric broadening of the pulse spectrum, self-steepening causes an asymmetry in the spectrum [23].

The NLS equation in this form has been successfully used to explain nonlinear effects in various media, notably in optical fibers [23]. This limited form of the

equation does not adequately explain the observed spectral broadening [6–9] and spatiotemporal dynamics [16–22] accompanying the propagation of intense laser pulses above the critical power for self-focusing. In addition, for powers above $P_{\rm cr}$, self-focusing leads to a spatial collapse of the beam into a singularity, which is unphysical. Thus, the model must include processes which arrest and halt catastrophic collapse. The high intensities created by self-focusing require that the onset of ionization be included in a more comprehensive model. Terms that capture the effect of the local plasma created due to ionization of gases, or transition of electrons from the valence band to the conduction band in the case of condensed matter, become necessary. As is common in literature, the term ionization is used for both these processes. At low intensities, below the threshold for nonlinear interactions, ionization or transition to the conduction band occurs by the absorption of a single photon of appropriate frequency and energy. When the central frequency of the pulse is less than what is required for resonant single photon absorption and ionization, at sufficiently high intensities, the availability of a surfeit of photons causes photoionization by the simultaneous absorption of more than one photon resulting in *multi-photon ionization* (MPI). An intense laser field also modifies the Coulomb potential barrier so that electrons can tunnel out of the bound state. As a result, *tunnel ionization* (TI) creates free electrons and contributes to the density of the local plasma. Electrons in the conduction band having sufficient kinetic energy can collide with electrons within the valence band causing them to make a transition to the conduction. They seed the process of *avalanche ionization* or *cascade ionization*. Keldysh [24] used the adiabaticity parameter (γ) to determine the dominant mechanism among tunneling ionization ($\gamma \ll 1$) and multi-photon ionization ($\gamma \gg 1$),

$$\gamma = \frac{\omega_0}{eE}(mU_i)^{1/2}. \tag{3}$$

Here ω is the laser frequency, m and e are the reduced mass and charge of the electron respectively, U_i the band gap and E the electric field. In our study the peak intensities do not exceed 10^{13} W cm^{-2}, the wavelength is 800 nm and the band gap U_i of BK-7 is 4.7 eV. The value of the Keldysh parameter in this case is 1.5. Following the Keldysh formulation [24–26], the photoionization rate is given by

$$W_{\rm PI}(|E|) = \frac{2\omega_0}{9\pi}\left(\frac{\omega_0 m}{\hbar\sqrt{\Gamma}}\right)^{3/2} Q(\gamma, x)\exp(-\alpha\langle x+1\rangle),$$

where $\Gamma = \gamma^2/(1+\gamma^2)$, $\Xi = 1-\Gamma$.

$$Q(\gamma, x) = \sqrt{\pi/2K\Xi}\sum_{n=0}^{\infty}\exp(-n\alpha)\Phi[\sqrt{\beta(n+2\nu)}],$$

where

$$\alpha = \pi\frac{K(\Gamma)-E(\Gamma)}{E(\Xi)}, \quad \beta = \frac{\pi^2}{4K(\Xi)E(\Xi)},$$
$$x = \frac{2}{\pi}\frac{U_i}{\hbar\omega_0}\frac{1}{\sqrt{\Gamma}}E(\Xi), \quad \nu = \langle x+1\rangle - x,$$

where $\langle \ldots \rangle$ denotes the integer part, K and E are complete elliptic integrals of the first and second kind and Φ is the Dawson integral, $\Phi(z) = \int_0^z \exp(y^2 - z^2)\mathrm{d}y$. Following Kennedy [27], the intensity-dependent photoionization rate can be simplified to

$$W_{\mathrm{PI}}(|E|) = A[BI]^k,$$

where

$$A = \frac{2\omega_0}{9\pi}\left(\frac{\omega_0 m}{\hbar\sqrt{\Gamma}}\right)^{3/2} \exp(2k)\Phi(z)(1/16)^k,$$

$$B = \frac{e^2}{m\omega_0^2 c\varepsilon_0 n_0 U_i}, \quad I = |E|^2. \tag{4}$$

k denotes the order of the multiphoton process and U_{i} the band gap/ionization potential. The process of photoionization at the rate W_{PI}, avalanche ionization and recombination contribute to the evolution equation for plasma electron density as described by the following rate equation [25,26]:

$$\frac{\partial \rho}{\partial t} = W_{\mathrm{PI}}(|E|) + \eta\rho|E|^2 - \rho/\tau_{\mathrm{r}}. \tag{5}$$

The avalanche ionization rate is given by $\eta = \sigma/U_{\mathrm{i}}$, *where* σ *is the coefficient of absorption due to inverse bremsstrahlung* $\sigma = \frac{k\omega_0\tau_{\mathrm{c}}}{n_0^2\rho_{\mathrm{c}}(1+\omega_0^2\tau_{\mathrm{c}}^2)} = 1.55 \times 10^{-18}$ cm^2, with collision time $\tau_{\mathrm{c}} = 2.33 \times 10^{-14}$ s, and $n_0^2\rho_{\mathrm{c}} = 2.3 \times 10^{21}$ cm^{-3} the critical density of the plasma. The last term in eq. (5) accounts for electron recombination with characteristic time of $\tau_{\mathrm{r}} = 150$ fs. Thus, the NLS equation extended to include the effects of ionization and the effects of the plasma electrons on the pulse envelope reads

$$\frac{\partial E}{\partial z} + \frac{i}{2}\beta_2\frac{\partial^2 E}{\partial t^2} - \beta_3\frac{\partial^3 E}{\partial t^3} - \frac{i}{2n_0k_0}\left(1 - \frac{i}{\omega_0}\frac{\partial}{\partial t}\right)\left(\frac{\partial^2}{\partial r^2} + \frac{1}{r}\frac{\partial}{\partial r}\right)E$$
$$= in_2k_0\left(1 + \frac{i}{\omega_0}\frac{\partial}{\partial t}\right)(|E|^2E) - \frac{\sigma}{2}(1 + i\omega_0\tau_{\mathrm{c}})\rho E - \frac{1}{2}\frac{W_{\mathrm{PI}}(|E|)U_{\mathrm{i}}\rho}{|E|^2}E. \tag{6}$$

In the present study, we start with a pulse Gaussian in space and secant hyperbolic in time with an envelope of the form

$$E(r, t, 0) = E_0 \exp(-r^2/w_0^2)\,\mathrm{sec}\,h(t/t_0). \tag{7}$$

The entry face of the BK-7 slab is considered as $z = 0$, where the beam is focused to a minimum waist $w_0 = 200$ μm, the temporal width of the pulse $t_0 = 100$ fs and the central wavelength $\lambda_0 = 800$ nm. The present study concentrates on spatio-temporal dynamics, i.e., the dynamics of the spatial profile and the temporal envelope. The studies of Kumagai *et al* [21], Couairon *et al* [25] and Chiron *et al* [22] justify retaining only the transverse Laplacian in the space-time focusing term for longer pulse widths, 100 fs or longer, when it is of interest to study only the spatio-temporal dynamics for pulses which are not in the few cycle limit. For the same reason we can ignore third-order GVD, self-steepening and Raman response.

With these considerations the extended NLS equation becomes (similar to refs [21] and [25]):

$$\frac{\partial E}{\partial z} + \frac{i}{2}\beta_2 \frac{\partial^2 E}{\partial t^2} - \frac{i}{2n_0 k_0}\left(\frac{\partial^2}{\partial r^2} + \frac{1}{r}\frac{\partial}{\partial r}\right) E$$
$$= in_2 k_0 |E|^2 E - \frac{\sigma}{2}(1 + i\omega_0 \tau_c)\rho E - \frac{1}{2}\frac{W_{PI}(|E|)U_i \rho}{|E|^2} E. \quad (8)$$

This considerably reduces the complexity of the problem and successfully replicates the important spatio-temporal features of the more complete equation. For BK-7 the other important parameters are $n_0 = 1.51$, $n_2 = 3.45 \times 10^{-16}$ cm^2/W and $\beta_2 = 0.0446$ fs$^2/\mu$m.

The code was written in MATLAB ® employing an operator-split technique for the solution of the resulting nonlinear parabolic equation. At each step in the z-direction, the field is determined in a two-step process. First, the terms involving the time operator are treated in the Fourier domain [23]. The spatial domain is integrated using a modified Crank–Nicholson scheme treating the nonlinear terms evaluated from the preceding step as source terms [27] and the plasma density obtained by second order Runge-Kutta integration of eq. (5).

3. Results and discussion

3.1 *Classification of propagation*

The dynamical spatio-temporal behavior of the intense femtosecond pulse is largely an interplay between diffraction, self-focusing, GVD, SPM and plasma effects. The most important factor governing the spatial dynamics is self-focusing which is a consequence of the Gaussian distribution of intensity of the pulse in a plane transverse to the propagation direction. Self-focusing overcomes the natural divergence due to diffraction for input powers greater than the critical power for self-focusing P_{cr}, which for a Gaussian pulse is given by [14,15]

$$P_{cr} = \frac{1.22\pi\lambda_0^2}{32 n_0 n_2}. \quad (9)$$

For BK-7, $P_{cr} = 1.75$ MW.

The collapse of the pulse due to self-focusing is arrested by a combination of GVD, SPM and by plasma formed by nonlinear photoionization. We have classified the study into three different regimes depending on the mechanism that arrests collapse and the different spatio-temporal characteristics which are a consequence of the interplay between self-focusing and the arresting mechanisms. For intensities just above P_{cr}, GVD combines with SPM to broaden [21] and split [28–30] the pulse temporally to prevent collapse and also the formation of appreciable plasma. The dynamics are governed entirely by GVD up to the threshold power for the formation of plasma P_{th} (defined in eq. (12)). Since GVD is the major player in the dynamics for input powers greater than P_{cr} but lesser than P_{th}, we call this the *GVD regime.*

When the initial input power is greater than the threshold power $P_{\rm th}$, the dominant mechanism for prevention of collapse is no more a combination of GVD and SPM alone. The underestimation of the width of the supercontinuum spectra when only GVD, SPM and self-steepening [21] alone are taken into account [31] and the fact that self-focusing distance is not correctly estimated without including the effects of the plasma created by the pulse [32], strongly suggest the role of the plasma in the dynamics at these powers. An appreciable local plasma is created by nonlinear photoionization for input powers greater than $P_{\rm th}$. GVD does not set in before self-focusing can create sufficient intensities to cause ionization in the medium leading to the formation of plasma. The plasma thus formed also counterbalances self-focusing and has a defocusing effect on the pulse, both spatially and temporally. In fact, the temporal defocusing or pulse broadening due to plasma electrons is very similar to that due to GVD. This has been observed by Gaeta [33] also. A dynamic balance reached between the two processes – self-focusing and the defocusing processes – leading to the formation of channel in which the beam travels as a filament without any appreciable change in its width for a distance several times its Rayleigh range, as was first observed by Braun *et al* [34]. Self-channeling is a characteristic of this regime. We call this the *ionization regime*. Further increase in the incident powers creates a strong plasma at very short propagation distances leading to the formation of multiple-cones with plasma effects completely dominating over all other processes that compete with self-focusing including diffraction. The manifestation of this under-dense plasma defines the *dominant plasma regime,* which for BK-7 begins at $100P_{\rm cr}$. Numerical studies on the dynamics in this regime for the case of BK-7 glass have not been performed hitherto to the best of our knowledge. We should emphasize that the results of experiments performed in this regime in BK-7 will be significantly different from those performed in other condensed media like quartz and fused silica because of the significant difference in the band gaps of these materials. The order of multiphoton ionization and the rate of avalanche ionization which depend on band gap, cause significant differences in the observed propagation dynamics in difference materials.

3.2 *GVD regime*

In media with normal dispersion, for input powers between $P_{\rm cr}$ and $P_{\rm th}$, collapse is prevented by dispersion. To set clear boundaries to the GVD regime, we define two characteristic lengths following definitive studies on self-focusing. The first of these is the *self-focusing length* $z_{\rm sf}$, which is the distance at which catastrophic collapse due to self-focusing occurs in the medium in the absence of an arresting mechanism. This is related to the pulse parameters by [35]

$$z_{\rm sf} = \frac{0.183\rho_0}{\sqrt{(\sqrt{P_0/P_{\rm cr}} - 0.852)^2 - 0.0219}}, \tag{10}$$

where $\rho_0 = \frac{\pi w_0^2 n_0}{\lambda}$. The variation of $z_{\rm sf}$ is plotted (dashed line) in figure 1a as a function of $p = P_0/P_{\rm cr}$, P_0 being the input power. The other characteristic length,

z_{nlgvd} [36], is the propagation distance over which the combined effects of GVD and SPM reduce the peak power from the input value to the critical power

$$z_{\mathrm{nlgvd}} \approx 0.5\rho_0 \left[\frac{\sqrt{3.38 + 5.2(p^2-1)} - 1.84}{15p\gamma}\right]^2, \tag{11}$$

where $\gamma = \rho_0/L_{\mathrm{dl}}$, $L_{\mathrm{dl}} = t_0^2/2\beta_2$ is the dispersion length. This is also plotted in figure 1a (dash-dot line) for the case of BK-7 and the pulse parameters are used here. The input powers for which p is between 1 and p_{th} constitute the GVD regime. Accordingly the threshold for plasma formation is

$$P_{\mathrm{th}} = p_{\mathrm{th}} P_{\mathrm{cr}}. \tag{12}$$

In the case of BK-7 for the pulse parameters considered here, $p_{\mathrm{th}} = 3.85$ and $P_{\mathrm{th}} = 3.85P_{\mathrm{cr}}$. The axial intensity for various powers leading up to P_{th} is shown in figure 1b. The peak increases and advances towards the input into the medium with increase in input power. Further, the collapse of the pulse into a singularity is prevented by pulse broadening and pulse splitting in GVD regime.

Gaeta [33] showed that collapse is arrested by pulse broadening due to dispersion, in the case of sapphire. The temporal splitting of the pulse occurs because self-focusing pushes the off-axis energy towards the center, $t = 0$. As the peak intensity increases, SPM also increases generating new frequencies. The nonlinear mixing of the frequencies induces a chirp along the pulse. The up- and down-shifted components grow in intensity and are eventually separated by normal dispersion as illustrated in figure 2a. This decreases the peak intensity and arrests collapse. This has indeed been observed in experiments [29,37]. In contrast to the symmetric splitting observed in the GVD regime, for powers greater than P_{th}, in the ionization regime, asymmetric splitting is observed due to the presence of plasma with the trailing edge having a lower intensity (figure 2b) as was observed by Diddams *et al* [29].

At input powers that fall within the limits of the GVD regime, the angular spectrum (λ vs. θ plots) can be explained using dispersion [38–40]. We find this to be the case in our simulations also. The input powers in this range are best-suited for pulse compression [41] and pulse shaping [42] since there is no distortion of the temporal profile of the pulse due to plasma which defocuses the trailing edge more strongly than the leading edge. Compression of pulses to a few optical cycles by proper dispersion management using appropriate initial chirp has been suggested and achieved [43].

3.3 *Ionization regime*

When the peak input power of the pulses is greater than the threshold power P_{th}, the self-focusing distance z_{sf} is smaller than z_{nlgvd} and collapse due to self-focusing cannot be halted by GVD. The large intensities generated trigger the nonlinear photoionization process bringing plasma into play. One or more narrow coherent structures – filaments are formed which propagate without divergence over several

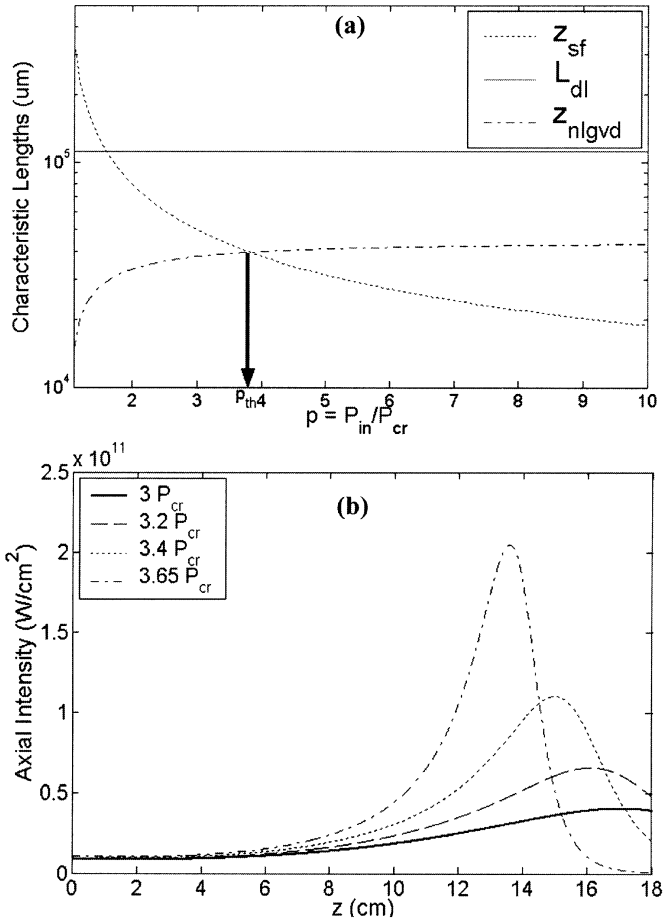

Figure 1. (**a**) Characteristic lengths for group velocity dispersion, self-focusing and the combined effect of SPM and GVD, for BK-7. (**b**) Variation of axial intensity ($|E(r = 0, t = 0)|^2$) with propagation distance, z, for various input powers in the GVD regime.

Rayleigh lengths. In atmosphere, such propagation up to several kilometers have been observed [44]. Such a beam with the transverse central maximum trapped is said to undergo *self-channeling* or *self-trapping*. The first observations of self-channeling with ultrashort pulses were by Braun *et al* [34], explained by a static balance between SF and plasma defocusing implying a soliton-like behavior both in space [26]. The long range dynamics was explained by Brodeur *et al* [45], using the *moving focus model*, in which the pulse is treated as consisting of longitudinal time slices which vary in intensity symmetrically on either side of $t = 0$. Slice by slice focusing then occurs at different values of z_{sf} depending on the power in the temporal slice.

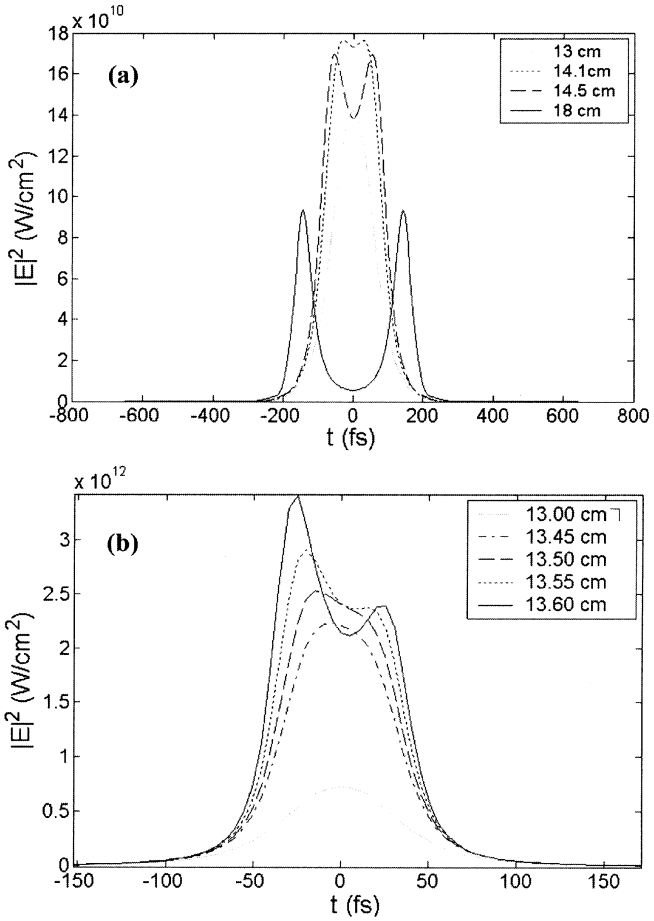

Figure 2. (**a**) Temporal splitting at the nonlinear focus for $3.85P_{\rm cr}$ and (**b**) for $5P_{\rm cr}$ along the axis ($r = 0$).

More detailed dynamics involve the interplay between the plasma created by the pulse, which in turn affects the pulse. The leading part of the pulse merely creates the plasma without being affected by it and hence will follow dynamics similar to the moving focus picture. The trailing part is defocused by the plasma generated by the leading edge. Pulses formed are absorbed and are subsequently replenished, causing the illusion of self-guiding viz., the *dynamic spatial replenishment model*. Numerical studies by Mlejnek *et al* [46] and Kosareva *et al* [47] have successfully used this model to explain important features observed in experiments ([45], [47] and references therein). Important features of the dynamics of the spatial replenishment are, the formation of a spatial ring formation due to on-axis plasma pushing the intensity peak off the center and subsequent refocusing. We use these to explain the asymmetric pulse splitting in this regime for BK-7. Recent developments point to the significant involvement of GVD in the filamentation observed in condensed media through nonlinear X-waves [40,48].

3.3.1 *Asymmetric pulse splitting and spatial replenishment.* In the case of BK-7, for powers greater but not too far from $P_{\rm th}$, asymmetric temporal splitting initially halts the collapse. This is a characteristic of the presence of plasma. The on-axis time profile at $5P_{\rm cr}$ shown in figure 2b illustrates this. The trailing edge is lower in intensity due to the defocusing by the plasma electrons which are left behind by the leading part of the pulse. The leading edge remains unaffected by these electrons. This leads to a marked skewness in the temporal profile, beginning at propagation distance of $z = 9.225$ cm. This change is accentuated by the formation of two pulses with unequal peaks at $z = 9.75$ cm. The on-axis splitting takes place because intensity is pushed away from the axis due to plasma formation leading to a spatial ring. On the axis now, there is not enough intensity to create plasma. The small temporal humps on either side of $t = 0$ begin to self-focus leading to a splitting. The intensity in the spatial rings is subsequently pushed back to the center, leading to on-axis refocusing as shown in figure 3. We note that such refocusing has also been reported in [19] and in the simulations of Kosareva *et al* [47] and Mlejnek *et al* [46]. This, indeed, is the spatial replenishment model at work. The experiment of Liu *et al* confirms the role of the off-axis energy [49]. When the off-axis energy is prevented from contributing to propagation by placing a limiting aperture, the effective propagation length of the filament is drastically reduced, thus highlighting the role of this background reservoir.

Further, from coefficients of the nonlinear photoionization term and the self-focusing term in the NLS equation, the intensity where the two effects balance out can be estimated as $I \sim (2n_2k_0/t_0\beta_4\sigma\tau_{\rm c}\omega\rho_0)^{1/3}$. For BK-7 this turns out to be $\sim 10^{12}$ W/cm^2. Our simulation concurs with this result when we note that this is the maximum intensity attained before temporal splitting is of the same order of magnitude (figure 2b). Intensity clamping of this kind has been observed in experiments in air [50] as well as in condensed matter [51].

3.3.2 *Self-channeling and filamentation.* Self-channeling, which is the hallmark of this regime, is explained by conventional models in which plasma supports channeling [34,36]. We replicated the numerical results of ref. [52] for propagation in air (figure 4) to validate the performance of our program in this regime. Since experimental results on channeling are concerned more with the observed spatial intensity profiles and much less the detailed internal temporal dynamics, we have chosen a macroscopic time averaged parameter indicative of the radius of the channeling. We define the channel radius by

$$r_{\rm ch} = \left\{ \frac{(\int_0^\infty r^2 F {\rm d}r)}{(\int_0^\infty F {\rm d}r)} \right\}^{1/2}, \tag{13}$$

where $F = \int_{-\infty}^{\infty} |E(r,t)|^2 {\rm d}t$, is the fluence.

For peak powers from $5P_{\rm cr}$ to $10P_{\rm cr}$ (figure 5), the channel radius is plotted as a function of the propagation distance obtained by integrating the NLS equation. Initially self-focusing reduces the beam radius, till it reaches a minimum radius after which the electron plasma defocuses the beam. For input powers up to $10P_{\rm cr}$, there is no channel formation and the behavior is similar to that observed in GVD regime where the beam diverges monotonically after reaching the nonlinear focus (see inset of figure 5). At $10P_{\rm cr}$, however, we clearly see the formation of a channel $\sim$2 cm long

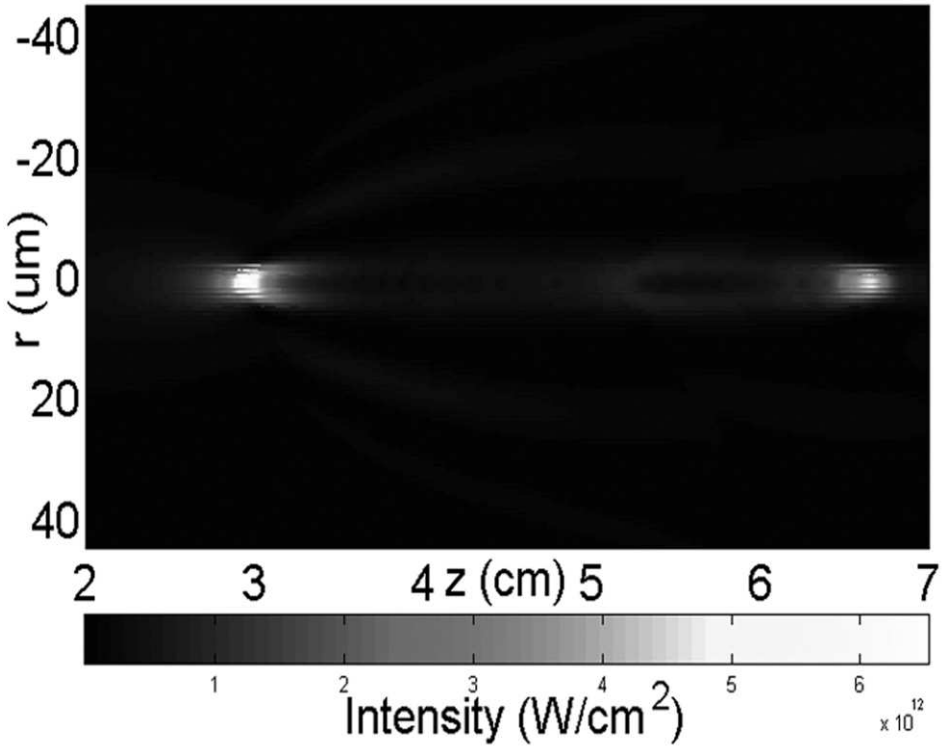

Figure 3. On-axis defocusing, subsequent refocusing of the pulse and spatial ring formation in the ionization regime.

figure 5. To get a complete picture of the dynamics we investigated channeling at higher powers in the range of $10P_{\rm cr}$ to $100P_{\rm cr}$. There was no qualitative difference in the dynamics of the time profile as both time-splitting and refocusing were observed. However, the spatial characteristics of the channel formed showed an interesting behavior. We define a parameter called the *channel length*, $L_{\rm ch}$, as the propagation distance over which the beam radius changes on either side of the point of minimum radius to $2^{1/2}$ of its minimum radius. This is similar to the definition of the Rayleigh range. Several methods, such as LIDAR, electromagnetic pulse emission, backward emitted nitrogen fluorescence and acoustic wave generation, have been proposed and comparatively studied for the measurement of channel length [53]. In figure 6a, we plot $L_{\rm ch}$ as a function of input power. The channeling distance steeply increases till $30P_{\rm cr}$, reaches a maximum and finally saturates to a value $\sim$3.5 cm. This can be explained by recognizing the role of GVD in arresting the collapse of the pulse. Though in the ionization regime GVD does not play an active role in the initial splitting as it does in the GVD regime, we may expect GVD to play a role in the post-focus dynamics.

To emphasize the importance of the role of GVD in plasma formation we performed the simulations using an artificial medium, in which all the parameters were the same as that for BK-7, except the GVD parameter which was chosen to be 100

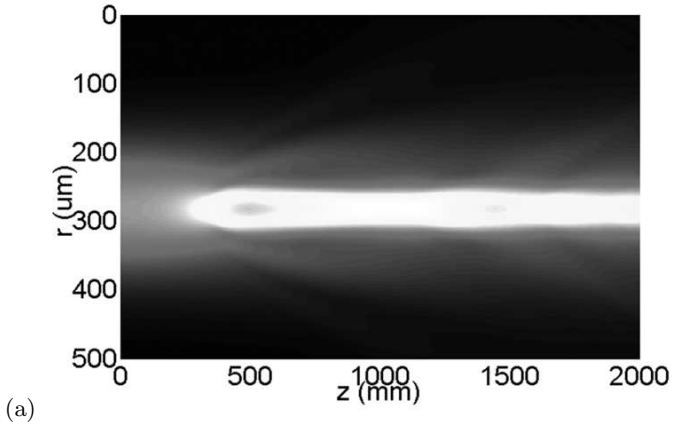

(a)

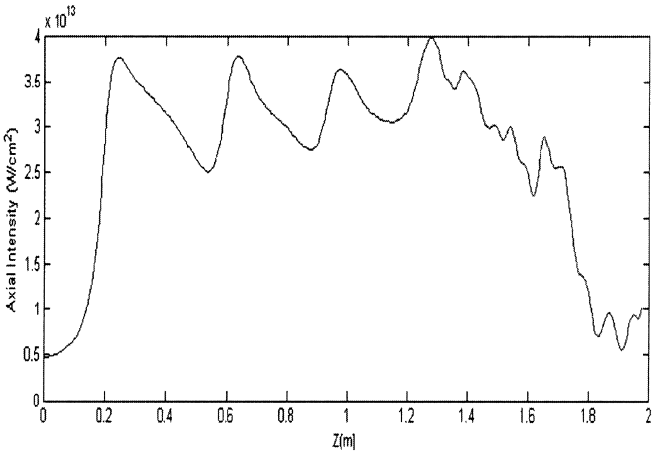

(b)

Figure 4. (**a**) Fluence and (**b**) on-axis intensity for propagation in air (parameters from ref. [46]).

times less. We expect channeling to start occurring for powers lower than $10P_{\rm cr}$ since the GVD parameter is lesser for the artificial medium. Indeed, in figure 7, we see that there is a prominent channeling at $7P_{\rm cr}$. We may recall that true BK-7 showed no channeling at $7P_{\rm cr}$ (figure 5). Secondly, the negligible amount of GVD in the artificial medium, manifests in the absence of any sharp rise followed by saturation (see inset of figure 7a) of the channel length as was observed in the case of true BK-7. These observations strongly suggest the continuing role of GVD in the post-focal dynamics and the propagation of the filament. These observations provide motivation for further experimental work in this regime. Indeed GVD has been shown to take over from ionization once again when the intensity is reduced to values close to $P_{\rm cr}$ as a consequence of ionization [54]. Recent work also suggests that the threshold for filamentation is lowered in amplifying media and a consequent increase in filament length as observed in a medium with a reduced GVD has been observed [55].

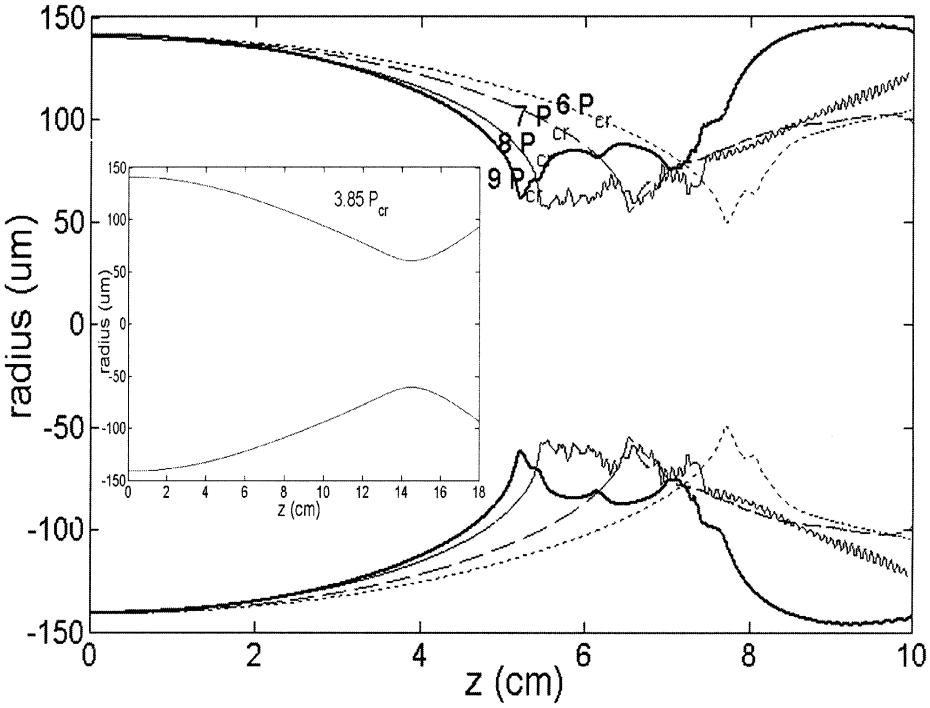

Figure 5. Variation of beam radius along the propagation axis, z, for input powers between 5 and $10P_{\rm cr}$. Inset shows the same for an input power of $3.85P_{\rm cr}$ which is in the GVD regime for BK-7.

The property of self-correction and self-healing of pulses at these input powers has been successfully used for self-cleaning of the transverse spatial mode of the beam [56]. Sustained propagation in atmospheric conditions and in the presence of aerosols has been experimentally demonstrated and modeled numerically [57]. Further, the permanent refractive index change consequent in bulk media on account of filamentation has been exploited in materials processing [58]. The use of filaments to compress pulses up to the single cycle limit [59] and their utility in obtaining tunable few-cycle pulses has been suggested [60]. In fact, advantages of using self-compression in filaments instead of the conventional hollow fiber to compress pulses down to few optical cycles have been evaluated by Wagner *et al* [61]. This regime lends itself naturally to several applications with a proper choice of input powers. Numerical studies prove to be a very effective method of choosing appropriate input energies. These observations motivate further experimental and numerical studies in this direction.

3.4 *Dominant plasma regime*

3.4.1 *Multiple-cone formation and guiding potentials.* The ionization regime extends from $P_{\rm th}$ ($= 3.85P_{\rm cr}$, for BK-7) onwards where filamentation is the key feature in the

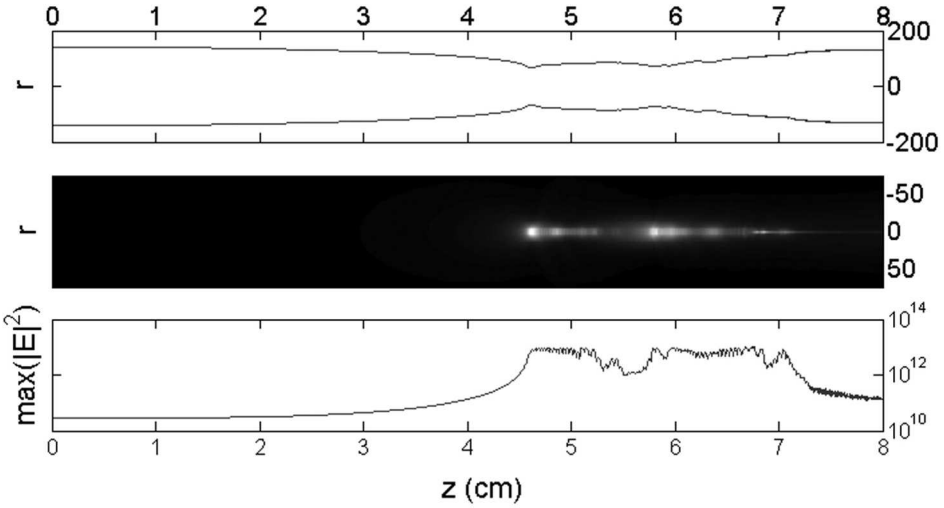

Figure 6. Self-channeling at $10P_{\rm cr}$. (Top) Variation of the $1/e$ point of the beam along the propagation axis, z. (Middle) The corresponding intensity plot. (Bottom) Fluence as a function of propagation distance.

propagation of the pulse. When the peak power is increased beyond $100P_{\rm cr}$ multiple cone structures are observed. This is a unique feature of the *dominant plasma regime*. This regime is typified by extreme defocusing by plasma leading to multiple cone formation. A strong plasma sets in early, before most other processes become appreciable and continues to dominate. In the GVD and ionization regimes we identified GVD and plasma, respectively, as the mechanisms which along with self-focusing govern the dynamics almost entirely in the respective regimes. Maintaining this approach to understanding the dynamics we point out the significant difference between the ionization regime and the dominant plasma regime using a method of ray potentials to examine the post-collapse dynamics [14]. We note that the diffraction term plays an important role in the dynamics. We examine the role of diffraction in this regime. GVD has no more significant role to play in the post-collapse dynamics.

We use the formalism of guiding potentials to analyze spatial effects at these high powers. In order to fix our attention to the spatial dynamics, we drop the other terms that affect only the temporal behaviour and those which are purely absorptive in nature – MPI and inverse bremsstrahlung. The NLS equation, eq. (5), becomes

$$\frac{\partial E}{\partial z} = \frac{i}{2n_0k_0}\left(\frac{\partial^2}{\partial r^2} + \frac{1}{r}\frac{\partial}{\partial r}\right)E + iP^{\rm nl}, \tag{14}$$

where the nonlinear term and the plasma term are grouped as

$$P^{\rm nl} = n_2k_0|E|^2E - \frac{\sigma}{2}\omega_0\tau_{\rm c}\rho E. \tag{15}$$

We adopt the analysis of propagation by using ray potentials [62]. The complex

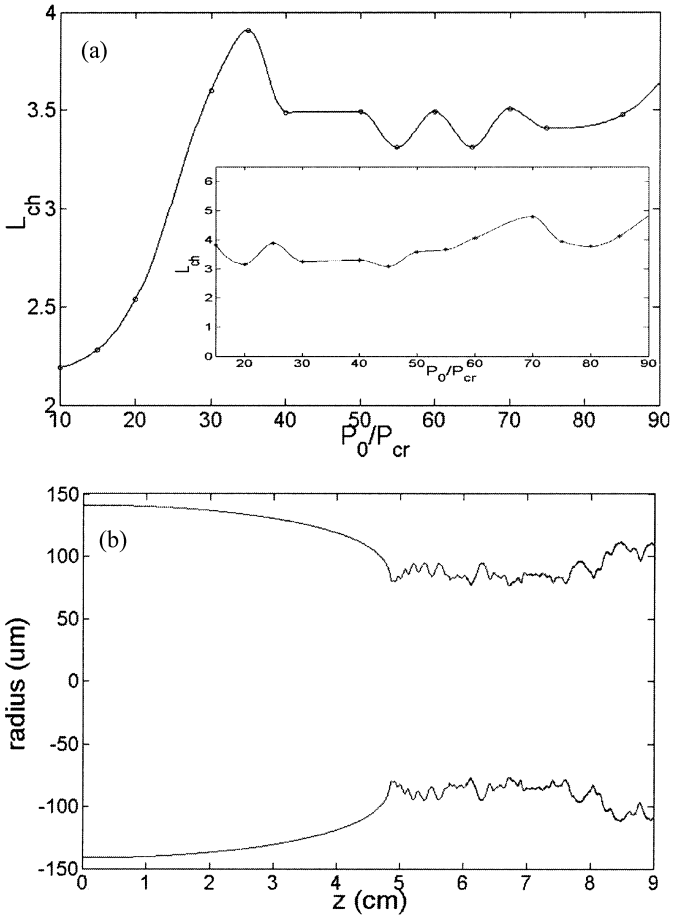

Figure 7. (**a**) Variation of channel length for BK-7 in the ionization regime, 10–90$P_{\rm cr}$. Inset shows the same for 'artificial BK-7'. (**b**) Formation of a channel for an input power of 7$P_{\rm cr}$ in the 'artificial' medium.

electric field for ray analysis can be written as $E = A\exp(iS)$, with A and S satisfying the equations

$$n_0 k_0 \frac{\partial A^2}{\partial z} + \nabla_{\rm T}(A^2 \nabla_{\rm T} S)E = 0,$$
$$2n_0 k_0 \frac{\partial S}{\partial z} + [\nabla_{\rm T} S]^2 - \frac{1}{A}[\nabla_{\rm T}^2 A] + P^{\rm nl} = 0. \tag{16}$$

The first equation is the power conservation equation in the transverse plane. The second equation of motion for the phase S has the form of a Hamilton–Jacobi equation [49] for the motion of a particle of unit mass moving in two dimensions under the influence of a *guiding potential*

$$U = -\frac{\nabla_{\mathrm{T}}^2 A}{2n_0^2 k_0^2 A} - \frac{n_2}{n_0} A^2 + n_{\mathrm{pl}}\rho \tag{17}$$

with $n_{\mathrm{pl}} = \sigma\omega_0\tau_{\mathrm{c}}/2n_0k_0$ where (n_0k_0z) is regarded as 'time', and (n_0k_0x) and (n_0k_0y) are treated as the spatial coordinates. The corresponding equation for the trajectories is

$$\frac{\mathrm{d}^2 r}{\mathrm{d}z^2} = -\nabla_{\mathrm{T}} U \tag{18}$$

from which the ray paths can be computed, if U is known as a function of x and y. U serves as a ray potential. We also define a diffractionless *auxiliary guiding potential* U' by

$$U' = -\frac{n_2}{n_0} A^2 + n_{\mathrm{pl}}\rho, \tag{19}$$

where the diffraction term has been removed. U' is U sans diffraction. An equation identical to (18) will define the ray paths in the case of U' also. We note that the ray propagation is allowed for regions where the potential function is attractive.

In figures 8a–d, we plot the ray potentials and auxiliary potentials for powers $30P_{\mathrm{cr}}$ and $400P_{\mathrm{cr}}$ just beyond their respective nonlinear foci. While $30P_{\mathrm{cr}}$ falls in the ionization regime, $400P_{\mathrm{cr}}$ is in the spatial splitting regime. It is clear from figures 8a and 8b that for $30P_{\mathrm{cr}}$ there is a marked difference between U and U'. Hence diffraction plays an important role in the dynamics at $30P_{\mathrm{cr}}$. On the contrary, at $400P_{\mathrm{cr}}$ (figures 8c and 8d), both U and U' are identical. The dynamics is thus wholly interplayed between self-focusing and plasma defocusing resulting in a new regime of propagation and diffraction effects are precluded by the early onset of plasma. Multiple cone formation is evident in the fluence profile, figure 9a, and the adjoining spatio-temporal plot of intensity (figures 9b and 9c). Experiments and simulations in air [63], quartz [21] and fused silica [64] at comparative powers reveal the universal nature of the cone formation. Thus, the formation of multiple cones is a characteristic of the high power regime. Indeed, the role of diffraction-like effects due to plasma which could terminate filaments has been suggested as a mechanism to understand recent experimental observations [65].

3.4.2 *Diffraction-like effects of plasma.* The analysis of the guiding potential with and without the diffraction term shows that at high powers the early onset of sufficiently strong plasma indeed precludes diffraction. This raises the question of how the self-focusing is counter-balanced. We show conclusively that the role of diffraction is taken over by plasma and diffraction-like effects due to plasma counter-balance self-focusing. We do this by using the analogue of the unit mass particle to arrive at the angle of the cone formed in the multiple-conformation.

In figures 10a and 10b, we plot the ray potentials at different time slices of the pulse at $z = 4000$ μm and $z = 5000$ μm. At $z = 4000$ μm, cone formation is at an incipient stage. The center of the pulse 'sees' an 'attractive' potential close to $r = 0$. The depth increases for the leading edge, $t = 0$ fs has a greater depth than $t = 70$ fs, indicating self-focusing. Self-focusing of the leading edge creates plasma, which defocuses the trailing part. The depth of the attractive potential decreases progressively becoming repulsive (i.e., positive valued) at $t = 600$ fs.

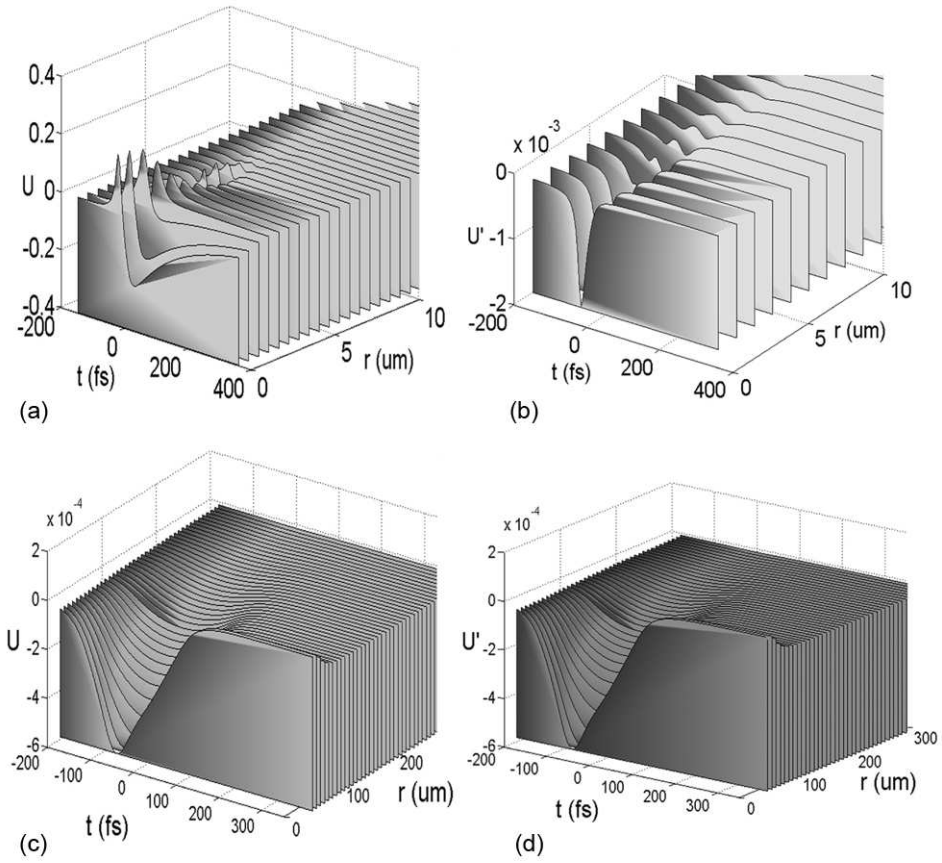

Figure 8. Spatio-temporal plots of (**a**) ray potential and (**b**) auxiliary potential at $30P_{\rm cr}$. (**c**) Ray potential and (**d**) auxiliary potential at $400P_{\rm cr}$.

At $z = 5000$ μm, again self-focusing is evident for the leading part, $t = -40$ fs. From $t = 0$ fs onwards, significant growth of plasma along the axis leads to intense defocusing, pushing the maximum of intensity away from the axis. The off-axis valley in the potential 'traps' the rays, forming a disk about the axis. This effect progresses as we move towards the trailing edge, $t = 0$, 70, 130 fs, pushing the intensity farther away from the axis till self-focusing is overcome completely by plasma defocusing, at the trailing end of the pulse. Thus the intensity in the wings grows at the expense of the center. This is evident in figure 10b where an off-axis 'valley' is seen in the potential curve for $t > 0$ within the pulse. This leads to a cone-like appearance in the propagation (figure 9a). Next, we show that the angle of the cone is directly related to the on-axis plasma density. This reinforces the fact that the auxiliary potential U' governs the dynamics and validates this approach. Conservation of total energy leads to a relation between change in the kinetic energy (T) and potential energy (V), $\delta T = -\delta V$. Here $T = 1/2(\mathrm{d}r/\mathrm{d}z)^2$

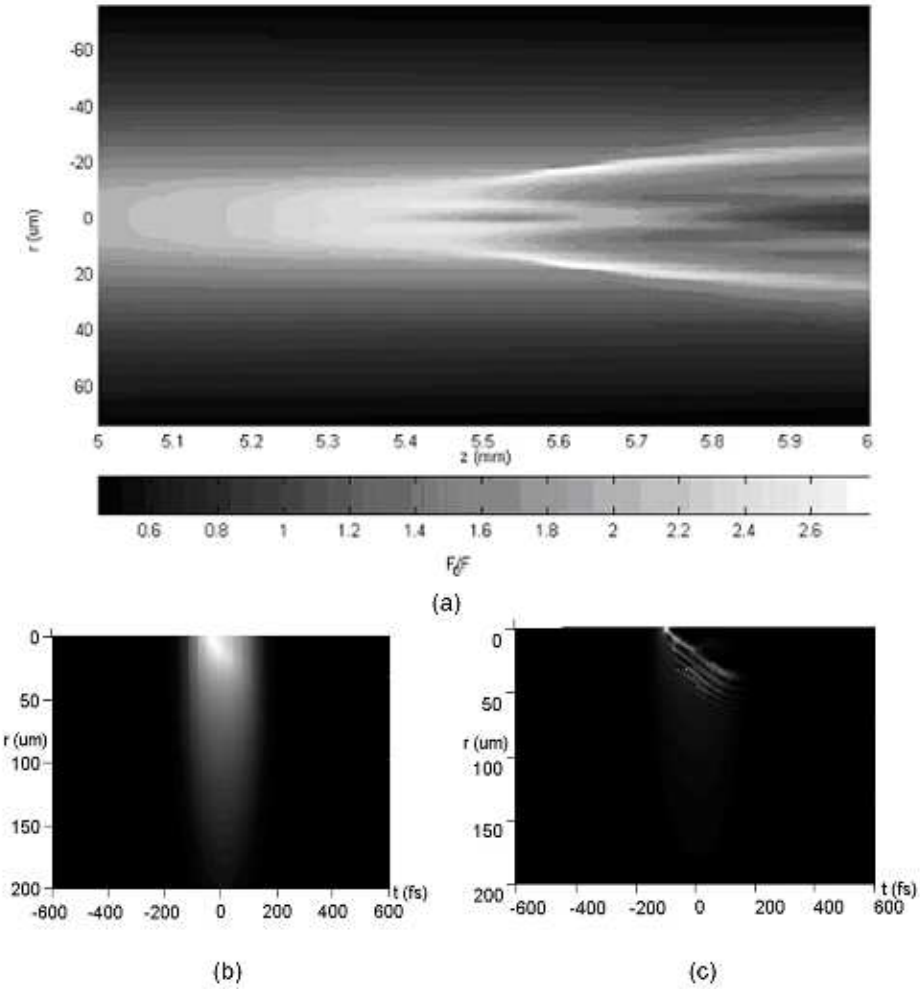

Figure 9. Fluence profile vs. z for $400P_{\rm cr}$ showing multiple cones, (**b**) spatio-temporal profile at a propagation distance of 5 mm and (**c**) at 6 mm.

is the kinetic energy of the particle of unit mass with the z-coordinate playing the role of time. At $r = 0$ the center of the cone, $\mathrm{d}r/\mathrm{d}z = 0$, which is evident from figure 10a. Hence, $1/2(\mathrm{d}r/\mathrm{d}z)^2 = \delta V$. In this case, we must consider the change in the auxiliary potential $\delta U'$ to compute δV. To compute $\delta U'$, we observe that U is a sum of two potentials, one responsible for self-focusing and the other due to plasma, $U' = U_{\rm sf} + U_{\rm pl}$ where, $U_{\rm sf} = (-n_2/n_0)A^2$ and $U_{\rm pl} = n_{\rm pl}\rho$. The contribution due to self-focusing gives U' an inverted bell-shape, as in figure 10b for a time $t = -40$ fs within the pulse. At a propagation distance of 6000 μm and $t = 0$ fs, the hump at $r = 0$ develops due to plasma defocusing (figure 10b). We can use the deviation from the inverted bell-shape as an estimate for δU in the vicinity of $r = 0$ and approximate $\delta U' \approx U_{\rm pl}(0)$. Therefore, $(\mathrm{d}r/\mathrm{d}z) = [2U_{\rm pl}(0)]^{1/2}$. But, $\mathrm{d}r/\mathrm{d}z$ is also

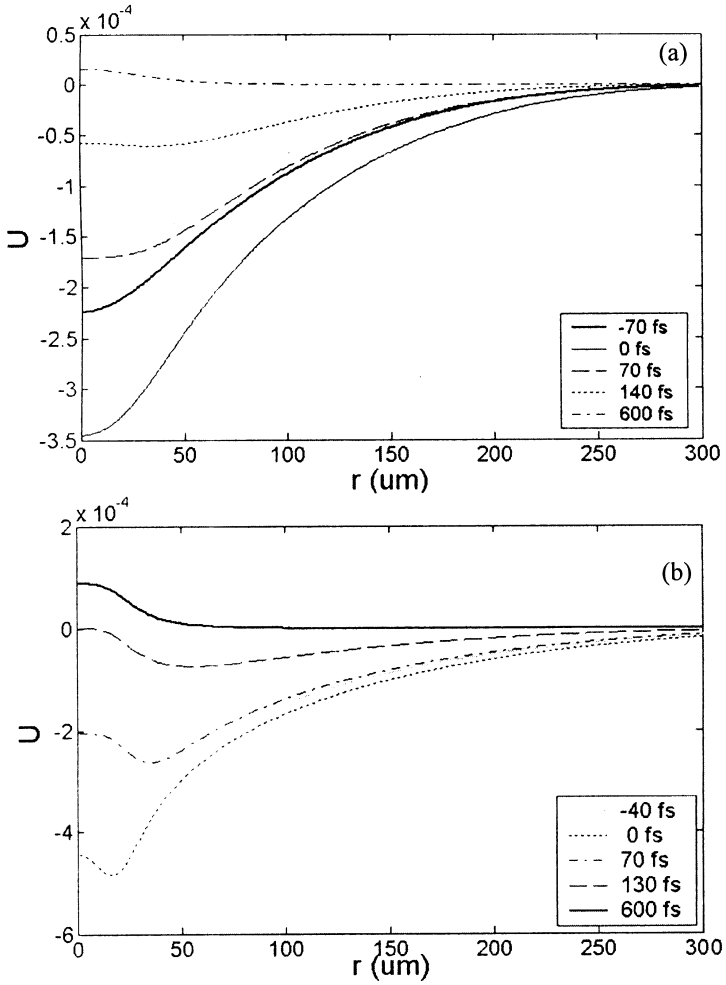

Figure 10. Ray potentials at different *intra-pulse* times at a propagation distance of (**a**) $z = 4$ mm and (**b**) at $z = 5$ mm for an input power of $400P_{\rm cr}$.

the angle of the cone, θ, in the cone structure formed. Using the peak intensity of the pulse at $z = 6000$ μm, we obtain $\theta = 0.12$ from this estimate. Alternatively, the cone angle can also be determined from the contour plot of the intensity of the pulse obtained by integrating the NLS equation. From the fluence profile, $\theta = 0.14$. The agreement between the two values of the cone angle – one obtained by integrating the NLS equation and that obtained from ray analysis – stands to validate our analysis further.

To the best of our knowledge, the direct relationship between the cone angle and on-axis plasma density has been demonstrated for the first time. This brings forth the important role of plasma at very high powers. The dominance of plasma on super-continuum spectra is also clear from the study of Dharmadhikari *et al* [66].

4. Conclusions

In this paper the propagation of an ultrashort laser pulse in a condensed medium (BK-7) has been studied over a wide range of input powers 1–1000P_{cr}. The dynamics has been neatly classified by identifying the most dominant mechanism that competes with self-focusing leading to a classification into three regimes – GVD, ionization and dominant plasma. All the important characteristics such as temporal splitting, self-channeling and multiple cone formation have been deduced by numerically solving the same equation over the entire range of powers. The direct relation between on-axis plasma density and the cone angle for very high powers has been brought out.

Acknowledgement

We are grateful to Dr A Couairon and Dr M Centurion for many illuminating discussions. We also gratefully acknowledge the referee for valuable suggestions towards improving the presentation of work in this paper.

References

[1] S Campbell, F C Dear, D P Hand and D T Reid, *J. Opt.* **A7**, 162 (2005)
[2] D Ashkenasi, G Muller, A Rosenfeld, R Stoian, I V Hertel, N M Bulgakova and E E B Campbell, *Appl. Phys.* **A77**, 223 (2003)
[3] J Kasparian, M Rodriguez, G Mejean, J Yu, E Salmon, H Wille, R Bourayou, S Frey, Y-B Andre, A Mysyrowicz, R Sauerbrey, J P Wolf and L Wöste, *Science* **301**, 61 (2003)
[4] P Rairoux, H Schillinger, S Niedermeier, M Rodriguez, F Ronneberger, R Sauerbrey, B Stein, D Waite, C Wedekind, H Wille, L Wöste and C Ziener, *Appl. Phys.* **B71**, 573 (2000)
[5] R R Alfano and S L Shapiro, *Phys. Rev. Lett.* **24**, 584 (1970)
[6] A K Dharmadhikari, F A Rajgara, N C Reddy, A S Sandhu and D Mathur, *Opt. Express* **12**, 695 (2004)
[7] N K M Naga Srinivas, S Sree Harsha and D Narayana Rao, *Opt. Express* **13**, 3224 (2005)
[8] H Schroeder, J Liu and S L Chin, *Opt. Express* **12**, 4768 (2004)
[9] A Dharmadhikari, F Rajgara, D Mathur, H Schroeder and J Liu, *Opt. Express* **13**, 8555 (2005)
[10] M R Kasaai, V Kacham, F Theberge and S L Chin, *J. Non-Crystalline Solids* **319**, 129 (2003)
[11] V Koubassov, J F Laprise, F Théberge, E Förster, R Sauerbrey, B Müller, U Glatzel and S L Chin, *Appl. Phys.* **A79**, 499 (2004)
[12] H B Sun, Y Xu, S Juodkazis, K Sun, M Watanabe, S Matsuo, H Misawa and J Nishii, *Opt. Lett.* **26**, 325 (2001)
[13] E N Glenzer, M Milojasavljevic, L Huang, R J Finlay, T H Her, J P Callan and E Mazur, *Opt. Lett.* **21**, 2023 (1996)
[14] J H Marburger, *Prog. Quantum Electr.* **4**, 35 (1975)

[15] R W Boyd, *Nonlinear Optics* (Academic Press, San Diego, 2003)
[16] M Hatayama, A Suda, M Nurhuda, K Nagasaka and K Midorikawa, *J. Opt. Soc. Am.* **B20**, 603 (2003)
[17] C Ren, B J Duda, R G Hemker, W B Mori, T Katsouleas, T M Antonsen Jr and P Mora, *Phys. Rev.* **E63**, 026411 (2001)
[18] S Tzortzakis, L Sudrie, M Franco, B Prade, A Mysyrowicz, A Couairon and L Bergé, *Phys. Rev. Lett.* **87**, 213902-1 (2001)
[19] W Liu, S L Chin, O Kosareva, I S Golubtsov and V P Kandidov, *Opt. Commun.* **225**, 193 (2003)
[20] W Liu, S A Hosseini, Q Luo, B Ferland, S L Chin, O G Kosareva, N A Panov and V P Kandidov, *New J. Phys.* **6**, 6 (2004)
[21] H Kumagai, S Cho, K Ishikawa, K Midorikawa, M Fujimoto, S Aoshima and Y Tsuchiya, *J. Opt. Soc. Am.* **B3**, 597 (2003)
[22] A Chiron, B Lamouroux, R Lange, J F Ripoche, M Franco, B Prade and G Bonnaud, *Eur. Phys. J.* **D6**, 383 (1999)
[23] G P Agarwal, in: The supercontinuum laser source edited by R R Alfano (Academic Press, San Diego, 1989)
[24] L V Keldysh, *Soviet Phys. JETP* **20**, 1307 (1965)
[25] A Couairon, L Sudrie, M Franco, B Prade and A Mysyrowicz, *Phys. Rev.* **B71**, 125435 (2005)
[26] P K Kennedy, *IEEE J. Quantum Electronics* **31**, 2241 (1995)
[27] J C Strikwerda, Finite difference schemes and partial differential equations (Wadsworth & Brooks/Cole Advanced Books & Software, California, 1989) ch. 7
[28] A A Zozulya, S A Diddams, A G Van Engen and T S Clement, *Phys. Rev. Lett.* **82**, 1430 (1999)
[29] S A Diddams H K Eaton, A A Zozulya and T S Clement, *Opt. Lett.* **23**, 379 (1998)
[30] M Nurhuda, A Suda, M Hatayama, K Nagasaka and K Midorikawa, *Phys. Rev.* **A66**, 023811 (2002)
[31] A Brodeur and S L Chin, *J. Opt. Soc. Am.* **B16**, 637 (1999)
[32] G Fibich, S Eisenmann, B Ilan, Y Erlich, M Fraenkel, Z Henis, A L Gaeta and A Zigler, *Opt. Express* **13**, 5897 (2005)
[33] A L Gaeta, *Phys. Rev. Lett.* **84**, 3582 (2000)
[34] A Braun, G Kohn, X Liu, D Du, J Squier and G Mourou, *Opt. Lett.* **20**, 73–75 (1995)
[35] J C Diels, W Rudolph, P F Liao and P Kelley, Ultrashort laser pulse phenomena (Academic Press, New York, 1996)
[36] G G Luther, J V Moloney and A C Newell, *Opt. Lett.* **19**, 862 (1994)
[37] J K Ranka, R W Schirmer and A L Gaeta, *Phys. Rev. Lett.* **77**, 3783 (1996)
[38] D Faccio, M A Porras, A Dubietis, G Tamosauskas, E Kucinskas, A Couairon and P Di Trapani, *Opt. Commun.* **265**, 672 (2006)
[39] P Di Trapani, G Valiulis, A Piskarskas, O Jedrkiewicz, J Trull, C Conti and S Trillo, *Phys. Rev. Lett.* **4**, 093904-1 (2003)
[40] M Kolesik, E M Wright and J V Moloney, *Phys. Rev. Lett.* **92**, 253901-1 (2004)
[41] S Champeaux and L Berge, *Phys. Rev.* **E68**, 066603 (2003)
[42] H Ward and L Berge, *Phys. Rev. Lett.* **90**, 053901-1 (2003)
[43] R Li, X Chen, J Liu, Y Leng, Y Zhu, X Ge, H Lu, L-H Lin and Z Xu, in *Laser resonators and beam control VIII* edited by A V Kudryashov and A H Paxton, *Proceedings of the SPIE 5708* (2005) vol. 5708, p. 102
[44] L Wöste, C Wedekind, H Wille, P Rairoux, B Stein, S Nikolov, C Werner, S Niedermeier, F Ronneberger, H Schillinger and R Sauerbrey, *Laser Optoelektronik* **29**, 51 (1997)

[45] A Brodeur, C Y Chien, F A Ilkov, S L Chin, O G Kosareva and V P Kandidov, *Opt. Lett.* **22**, 304 (1997)
[46] M Mlejnek, E M Wright and J V Moloney, *Opt. Lett.* **23**, 382 (1998)
[47] O G Kosareva, V P Kandidov, A Brodeur, C Y Chien and S L Chin, *Opt. Lett.* **22**, 1332 (1997)
[48] A Couairon, E Gaižauskas, D Faccio, A Dubietis and P Di Trapani, *Phys. Rev.* **E73**, 016608 (2006)
[49] W Liu, F Théberge, E Arévalo, J-F Gravel, A Becker and S L Chin, *Opt. Lett.* **30**, 2602 (2005)
[50] A Becker, N Akozbek, K Vijayalakshmi, E Oral, C M Bowden and S L Chin, *Appl. Phys.* **B73**, 287 (2001)
[51] W Liu, S Petit, A Becker, N Akozbek, C M Bowden and S L Chin, *Opt. Commun.* **202**, 189 (2002)
[52] A Couairon, *Phys. Rev.* **A68**, 015801 (2003)
[53] S A Hosseini, J Yu, Q Luo and S L Chin, *Appl. Phys.* **B79**, 519 (2004)
[54] S Champeaux and L Berge, *Phys. Rev.* **E71**, 046604 (2005)
[55] J Philip, C D'Amico, G Chériaux, A Couairon, B Prade and A Mysyrowicz, *Phys. Rev. Lett.* **95**, 163901 (2005)
[56] B Prade, M Franco, A Mysyrowicz, A Couairon, H Buersing, B Eberle, M Krenz, D Seiffer and O Vasseur, *Opt. Lett.* **31**, 2601 (2006)
[57] S Skupin, L Bergé, U Peschel and F Lederer, *Phys. Rev. Lett.* **93**, 023901-1 (2004)
[58] S-H Cho, H Kumagai and K Midorikawa, *Appl. Phys.* **A76**, 755 (2003)
[59] A Couairon, J Biegert, C P Hauri, W Kornelis, F W Helbing, U Keller and A Mysyrowicz, *J. Mod. Opt.* **53**, 75 (2006)
[60] F Theberge, N Akozbek, W Liu, A Becker and S L Chin, *Phys. Rev. Lett.* **97**, 023904 (2006)
[61] N L Wagner, E A Gibson, T Popmintchev, I P Christov, M M Murnane and H C Kapteyn, *Phys. Rev. Lett.* **93**, 173902-1 (2004)
[62] M Born and E Wolf, *Principles of Optics* 6th edition (Cambridge University Press, London, 1997) ch. 3
[63] S L Chin, N Akozbek, A Proulx, S Petit and C M Bowden, *Opt. Commun.* **188**, 181 (2001)
[64] K Ishikawa, H Kumagai and K Midorikawa, *Phys. Rev.* **E66**, 056608 (2002)
[65] W Liu, Q Luo, F Théberge, H L Xu, S A Hosseini, S M Sarifi and S L Chin, *Appl. Phys.* **B82**, 373 (2006)
[66] A K Dharmadhikari, F A Rajgara and D Mathur, *Appl. Phys.* **B82**, 575 (2006)